JACS
JOURNAL OF THE AMERICAN CHEMICAL SOCIETY
Article
pubs.acs.org/JACS

Mechanistic Insights into C−H Oxidations by Ruthenium(III)-Pterin Complexes: Impact of Basicity of the Pterin Ligand and Electron Acceptability of the Metal Center on the Transition States

Hiroumi Mitome,[†] Tomoya Ishizuka,[†] Hiroaki Kotani,[†] Yoshihito Shiota,[‡] Kazunari Yoshizawa,[‡] and Takahiko Kojima*[,†]

[†]Department of Chemistry, University of Tsukuba, 1-1-1 Tennoudai, Tsukuba, Ibaraki 305-8571, Japan
[‡]Institute for Materials Chemistry and Engineering, Kyushu University, Motooka, Nishi-Ku, Fukuoka 819-0395, Japan

Supporting Information

ABSTRACT: A ruthenium(II) complex, [Ru(dmdmp)Cl(MeBPA)] (**2**) (Hdmdmp = *N*,*N*-dimethyl-6,7-dimethylpterin, MeBPA = *N*-methyl-*N*,*N*-bis(pyridylmethyl)amine), having a pterin derivative as a proton-accepting ligand, was synthesized and characterized. Complex **2** shows higher basicity than that of a previously reported Ru^{II}-pterin complex, [Ru(dmdmp)(TPA)]$^+$ (**1**) (TPA = tris(2-pyridylmethyl)amine). On the other hand, 1e$^-$-oxidized species of **1** ($\mathbf{1}_{OX}$) exhibits higher electron-acceptability than that of 1e$^-$-oxidized **2** ($\mathbf{2}_{OX}$). Bond dissociation enthalpies (BDE) of the two Ru^{II} complexes having Hdmdmp as a ligand in proton-coupled electron transfer (PCET) to generate $\mathbf{1}_{OX}$ and $\mathbf{2}_{OX}$ were calculated to be 85 kcal mol^{-1} for $\mathbf{1}_{OX}$ and 78 kcal mol^{-1} for $\mathbf{2}_{OX}$. The BDE values are large enough to perform H atom transfer from C−H bonds of organic molecules to the 1e$^-$-oxidized complexes through PCET. The second-order rate constants (k) of PCET oxidation reactions were determined for $\mathbf{1}_{OX}$ and $\mathbf{2}_{OX}$. The logarithms of normalized k values were proportional to the BDE values of C−H bonds of the substrates with slopes of −0.27 for $\mathbf{1}_{OX}$ and −0.44 for $\mathbf{2}_{OX}$. The difference between $\mathbf{1}_{OX}$ and $\mathbf{2}_{OX}$ in the slopes suggests that the transition states in PCET oxidations of substrates by the two complexes bear different polarization, as reflection of difference in the electron acceptability and basicity of $\mathbf{1}_{OX}$ and $\mathbf{2}_{OX}$. The more basic $\mathbf{2}_{OX}$ attracts a proton from a C−H bond via a more polarized transition state than that of $\mathbf{1}_{OX}$; on the contrary, the more electron-deficient $\mathbf{1}_{OX}$ forms less polarized transition states in PCET oxidation reactions of C−H bonds.

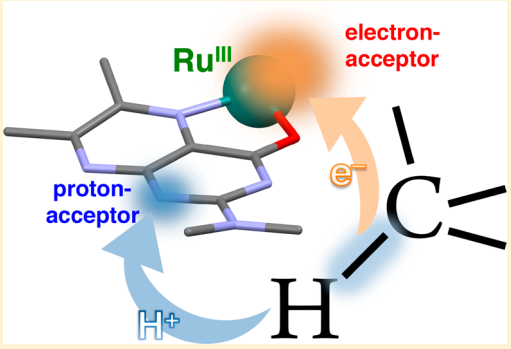

INTRODUCTION

Proton-coupled electron transfer (PCET) provides an energetically feasible pathway for H atom abstraction from compounds having an H atom.[1] In PCET reactions, an oxidant receives one electron and one proton from substrates at different sites; i.e., an electron goes to an electron-accepting redox-active site and a proton moves to a proton-accepting basic site.[2] The concerted processes reduce activation free-energy, $\Delta G^{\ddagger}$, in oxidation of hydrocarbons despite their high oxidation potentials (normally, >2 V vs SCE).[1b] Because of this advantage, PCET reactions are widely employed not only in biological redox reactions but also in production of fine chemicals in chemical industry.[3,4] In biological systems, oxidation reactions through a PCET process are also conducted at an active center by oxidation enzymes;[5] for example, lipoxygenase,[6] methane monooxygenase,[7] ribonucleotide reductase,[8] and cytochrome P450s[9] oxidize organic substrates at their active sites including transition metal complexes. The active sites of the enzymes are well characterized, and many research groups have synthesized transition metal complexes as functional models to gain mechanistic insights into the enzymatic oxidation reactions and to learn excellent methods for oxidation of organic molecules.[5,10−12]

PCET reactions can be categorized into 4 types; (1) electron transfer followed by proton transfer (ET/PT), (2) proton transfer followed by electron transfer (PT/ET), (3) concerted proton−electron transfer (CPET) to different electron- and proton-accepting sites, and (4) hydrogen atom transfer (HAT), in which a proton and an electron are concertedly transferred from a substrate to one site of the oxidant such as an oxyl group.[1b,13] In CPET reactions, the "oxidation power" of an oxidant can be defined by the bond dissociation enthalpy (BDE) of a 1e$^-$/1H$^+$-reduced form of the oxidant.[14] Also, the inertness of a substrate in HAT can be judged from the BDE value of an X-H bond to be cleaved. BDE values of the reduced species obtained from oxidants are determined from the pK_a value of its conjugate acid and the redox potential ($E_{1/2}$),[15] which correspond to the Gibbs free-energy change of the PCET reaction. The BDE value can be defined by eq 1:[16−19]

Received: April 12, 2016
Published: July 12, 2016

DOI: 10.1021/jacs.6b03785
J. Am. Chem. Soc. 2016, 138, 9508−9520

$$\text{BDE (kcal mol}^{-1}) = 2.303RT(\text{p}K_a) + F(E_{1/2}) + C \quad (1)$$

In eq 1, R, F, $E_{1/2}$ and C refer to the gas constant, the Faraday constant, one-electron oxidation potential, and a proportionality constant in a certain solvent, respectively. Thus, the high pK_a and high E_{red} values result in high BDE of the reduced species obtained from the oxidant to promote the oxidation reaction. The correlation between the oxidation reactivity of an oxidant and the BDE value of an oxidant as a hydrogen-atom acceptor has been well investigated by many researchers mainly with high-valent metal-oxo complexes as an oxidant.[20] In high-valent metal-oxo species, the oxo groups of the oxidants can behave as good proton acceptors by virtue of their −2 charge, and the metal centers can act as good electron acceptors based on their high valency. Therefore, many researchers have used metal-oxo species in CPET reactions. As an example of the reports investigating PCET reactivity of metal-oxo complexes, Que, Shaik, Nam and co-workers compared reactivity among nonheme iron(IV)-oxo complexes showing close calculated BDE values to each other in C−H abstraction reactions, to conclude that the involvement of the quintet state of iron(IV)-oxo complexes should be important in enhancing the reactivity of H atom abstraction.[21] As mentioned above, an important factor to determine the reactivity of an oxidant for the PCET reaction is its BDE value, which can be divided into two components, i.e., pK_a and $E_{1/2}$. Determination of reduction potential values (E_{red}) of metal-oxo complexes is relatively easy, and thus correlation between the E_{red} value and the reactivity as an oxidant has been discussed for several metal-oxo complexes;[22] for example, Que and co-workers determined the reduction potential of $[Fe^{IV}(O)(N4Py)]^{2+}$ (+0.50 V vs SCE in MeCN) by spectropotentiometry,[11] and concluded that the higher reactivity of $[Fe^{IV}(O)(N4Py)]^{2+}$ than Fe^{IV}-oxo-tetramesityl-porphyrin (+0.29 V)[23] and Fe^{IV}-oxo-trisureaylate (−0.06 V)[24] was attributed to its high potential among the Fe^{IV}-oxo complexes.[11] On the other hand, the correlation between pK_a of oxidants and its reactivity in C−H oxidation has never been clarified yet, due to the difficulty in the determination of pK_a values of metal-oxo species,[25] because metal-oxo complexes are generally unstable and usually not capable of accepting a proton in an acid−base reaction.

Besides the C−H oxidation by metal-oxo complexes mentioned above, no report has described systematic investigation on C−H oxidation reactions with metal complexes without oxo ligands.[26] Mayer and co-workers have reported that PCET oxidation of O−H bonds in substrates such as phenol derivatives and TEMPOH can be achieved by using Ru(III) and Fe(III) complexes having basic sites in the ligands without oxo ligands.[27,28] It should be important to develop oxidants without oxo ligands for expansion of versatility in C−H oxidation reactions: This strategy may allow us to construct catalytic oxidation systems without using hazardous peroxides to form metal-oxo complexes.

In order to clarify controlling factors of the reactivity of oxidants in C−H bond cleavage via CPET, we examined metal complexes bearing a basic site as a proton-accepting site, without oxo ligands. As a proton-accepting site, we chose a pterin derivative as a ligand. Pterins are heteroaromatic coenzymes, which play crucial roles in biological redox reactions.[29,30] Additionally, transition metal complexes of pterin derivatives have attracted much attention to shed light on the unique redox behavior in biological systems.[31,32] In our previous report, the 1e$^-$-oxidized species of a Ru^{II}-pterin complex, $[Ru^{II}(dmdmp)(TPA)]^+$ (**1**: Hdmdmp = *N*,*N*-dimethyl-6,7-dimethylpterin, TPA = tris(2-pyridylmethyl)-amine; see Scheme 1),[33] was revealed to perform oxidation reactions of phenol derivatives through a CPET mechanism;[34] however, H atom abstraction reactions from C−H bonds have never been performed. In this work, a novel ruthenium(II)-pterin complex, $[Ru^{II}(dmdmp)Cl(MeBPA)]$ (**2**: MeBPA = *N*-methyl-*N*,*N*-bis(2-pyridylmethyl)amine; see Scheme 1), has been synthesized: Complex **2** has a similar structure to that of **1**, except possession of a chloride ligand, instead of one pyridine ring of the TPA ligand in **1**. The alteration of coordination environments between **1** and **2** involves differences in total charges of the cation moieties, the pK_a values of the pterin ligand and 1e$^-$-oxidation potentials of the metal centers to regulate the reactivity of the complexes in PCET reactions. We herein compare the reactivity of 1e$^-$-oxidized **1** and **2** in oxidation of organic substrates, involving H atom abstraction from C−H bonds of substrates, to explore the effect of the differences in the electron-acceptability reflected on the redox potentials and the basicity reflected on the pK_a values between **1** and **2** on the substrate oxidation through a PCET mechanism. The purpose of this study is (1) clarification of the fact that nonmetal-oxo oxidants having proton- and electron-accepting sites are capable of performing sufficient C−H bond oxidation and (2) gaining insights into impacts of basicity and electron acceptability of the oxidants on the transition states in PCET oxidation reactions of C−H bonds.

Scheme 1. Structures of Complexes 1 and 2

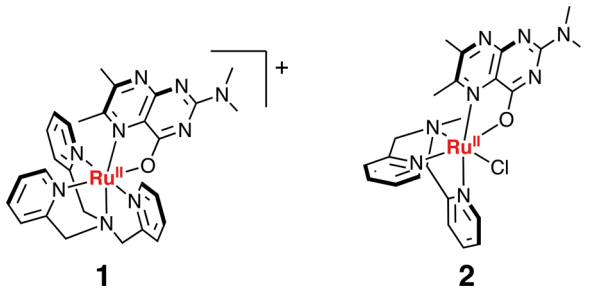

1 **2**

EXPERIMENTAL SECTION

General Methods. All chemicals available were purchased from appropriate commercial sources and used as received without further purification unless otherwise mentioned. MeBPA,[35,36] Hdmdmp[37] and $[Ru^{II}(dmdmp)(TPA)](ClO_4)$[33] were prepared according to literature procedures. $[Ru^{III}Cl_3(MeBPA)]$ was prepared using a modified procedure reported by Shimizu et al.[38] 9,10-Dihydro-anthracene-d_4 (DHA-d_4) was prepared according to a method reported by Goldsmith et al.[39]

All NMR measurements were performed using a JEOL JMN-ECS 400 spectrometer at room temperature. ESI-TOF- and GC-EI-MS spectra were measured on JEOL JMS-T100CS and SHIMADZU GC-2010 Plus spectrometers, respectively. UV−vis absorption spectra were recorded on Shimadzu UV-3600 and -2450 spectrophotometers. Electrochemical measurements were made using a BAS CV-1B electrochemical analyzer in freshly distilled MeCN containing 0.1 M tetrabutylammonium hexafluorophosphate ($TBAPF_6$) as an electrolyte. A small three-electrode cell (2.0 mL) was used with a platinum-disk working electrode and a platinum wire as a counter electrode. The potentials were measured with respect to an $Ag/AgNO_3$ reference electrode and all of the potentials were calibrated with ferrocene/ferrocenium (+0.40 V vs SCE in MeCN[40]) and then converted to values versus SCE by adding +0.40 V. All electrochemical measurements were carried out under an atmospheric pressure of Ar at room

DOI: 10.1021/jacs.6b03785
J. Am. Chem. Soc. 2016, 138, 9508−9520

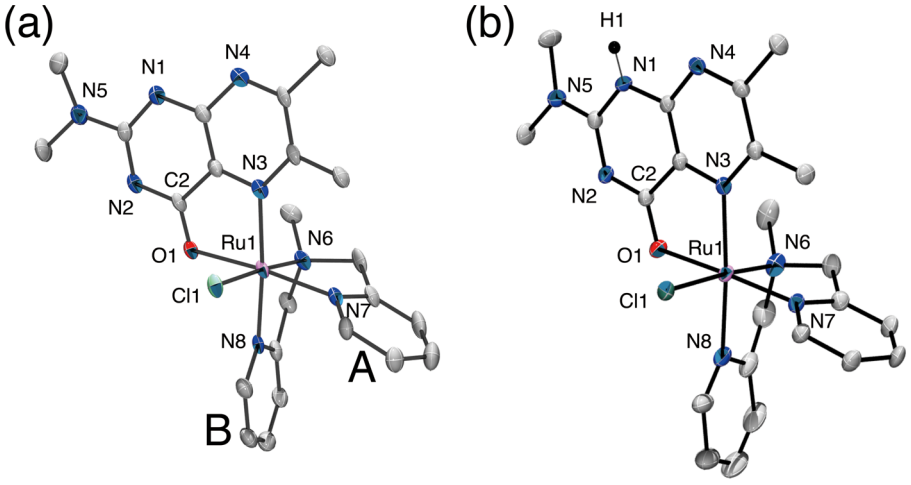

Figure 1. ORTEP drawings of (a) **2** and (b) **2**-H$^+$ with thermal ellipsoids at the 50% probability level. Pyridine rings of **2** are labeled as "A" and "B" to clarify assignments of ^{1}H NMR signals in the Experimental Section.

temperature. ESR spectra were recorded on a Bruker EMXPlus 9.5/2.7 spectrometer at room temperature or 100 K under Ar.

Kinetic Analyses of Substrate Oxidations. Kinetic studies of substrate oxidation reactions with $\mathbf{1}_{OX}$ or $\mathbf{2}_{OX}$ were performed on a UNISOKU USP-SFM-CRD10 stopped-flow spectrometer equipped with a multichannel photodiode array using a double-mixing mode at 296 K in superdehydrated grade MeCN (Wako Pure Chemical Industries) as a solvent. Ru^{II}-dmdmp complexes (**1** or **2**: 15 μM) were treated with $[Fe^{III}(bpy)_3](PF_6)_3$ (15 μM) to generate the corresponding Ru^{III}-dmdmp complexes ($\mathbf{1}_{OX}$ and $\mathbf{2}_{OX}$). After an incubation time of 1.0 s, substrates were added to the solution. The spectral changes were monitored by the rise of the absorption band centered at 530 nm due to the formation of Ru^{II}–Hdmdmp complexes (**1**-H$^+$ and **2**-H$^+$). The kinetic measurements were carried out at 296 K under pseudo-first-order conditions, where the concentrations of the substrates were set to be more than 100-fold excess to the Ru^{III}-dmdmp complexes. Pseudo-first-order rate constants (k_{obs}) were determined by least-squares curve fittings for the absorbance changes at 530 nm on the basis of eq 2:

$$A = A_\infty \exp(1 - k_{obs}t) \quad (2)$$

where A and A_∞ refer to the absorbance at 530 nm at the moment of t and at the infinite time after the initiation of the reaction. A linear fit to the plot of the k_{obs} values obtained against the concentration of the substrate gave the second-order rate constant, k, as the slope (eq 3).

$$k_{obs} = k[\text{substrate}]_0 \quad (3)$$

*Synthesis of [Ru(dmdmp)Cl(MeBPA)] (**2**).* To a mixture of $[Ru^{III}Cl_3(MeBPA)]$ (56.6 mg, 135 μmol) and Hdmdmp (32.5 mg, 148 μmol) was added ethanol (48 mL), and then water (12 mL) was poured into the suspension. The mixture obtained was degassed and heated at reflux under Ar. Color change of the mixture from brown to dark red was observed immediately after heating, and further reflux for 12 h gave a dark purple solution. This solution was filtered and Et_3N (10 mL, 72 mmol) was added to the filtrate. EtOAc (150 mL) was added to the red solution obtained and the mixture was concentrated to half a volume to give brown suspension. Filtration of the suspension gave brown powder and colorless needles, the latter of which were assumed to be $(Et_3NH)Cl$. The solid mixture was dissolved into methanol, and the target compound was separated with column chromatography on Sephadex LH20 eluted with MeOH. The first dark-red fraction was collected, and further purification was performed with column chromatography on Sephadex LH20 eluted with MeOH to remove the protonated species (**2**-H$^+$). After adding EtOAc into the fraction, the solution was concentrated to give dark purple solution with brown powder. The suspension was filtered, and the obtained solid was washed with EtOAc and diethyl ether gave the target compound as brown powder (30.6 mg, 53.8 μmol, 40%). Anal.: Calcd for $C_{23}H_{27}N_8OClRu\cdot0.5H_2O\cdot0.5MeOH$: C 47.59, H 5.10, N 18.89; Found: C 47.87, H 4.84, N 18.91. ESI-TOF-MS (MeOH): m/z = 591.1 (calcd. for $\{Na^+ + [Ru^{II}(dmdmp^-)Cl^-(MeBPA)]\}^+$: 591.2). ^{1}H NMR ($CD_3CN$): δ 2.12 (s, 3H, 7-Me), 2.18 (s, 3H, CH_3 of MeBPA), 2.23 (s, 3H, 6-Me), 2.52 (s, 6H, NMe_2), 3.89–4.12 (m, 4H, CH_2), 7.03 (ddd, 1H, J = 7.7, 5.8, 1.2 Hz, H5 of pyridine-A), 7.06 (dd, 1H, J = 7.7, 1.2 Hz, H3 of pyridine-A), 7.15 (ddd, 1H, J = 7.7, 6.3, 1.1 Hz, 5H of pyridine-B), 7.23 (dd, 1H, J = 7.2, 1.1 Hz, H3 of pyridine-B), 7.39 (td, 1H, J = 7.7, 1.2 Hz, H4 of pyridine-A), 7.57 (ddd, 1H, J = 7.7, 7.2, 1.1 Hz, H4 of pyridine-B), 9.46 (dd, 1H, J = 5.8, 1.2 Hz, H4 of pyridine-A), 9.56 (dd, 1H, J = 6.3, 1.1 Hz, H6 of pyridine-B). UV–vis (MeCN): λ_{max} [nm] (ε [M^{-1} cm^{-1}]) = 392 (1.4×10^4), 495 (9.1×10^3).

Synthesis of [RuCl(Hdmdmp)(MeBPA)](PF$_6$) (2-H$^+$·PF$_6$). Recrystallization of crude **2**-H$^+$, which was prepared by the method mentioned above, from acetone/octane in the presence of NH_4PF_6, gave dark purple crystals. Anal.: Calcd for $C_{23}H_{28}N_8OF_6PClRu$: C 38.69, H 3.95, N 15.69; Found: C 38.97, H 3.94, N 15.38. ESI-TOF-MS (MeOH): m/z = 569.1 (calcd. for $\{[Ru^{II}Cl^-(Hdmdmp)(MeBPA)]\}^+$: 569.1). UV–vis (MeCN): λ_{max} [nm] (ε [M^{-1} cm^{-1}]) = 326 (1.6×10^4), 363 (1.4×10^4), 549 (9.4×10^3).

Synthesis of 1,2,3,4,5-Pentamethyl-cyclopentadiene-d$_1$ (HCp-d$_1$).* 1,2,3,4,5-Pentamethyl-cyclopentadiene (500 μL, 3.19 mmol) was dissolved into distilled THF (5 mL) under Ar, and 1.6 M solution of *n*-BuLi in hexane (5 mL) was added. The solution immediately turned to gel, and D_2O was added into the mixture. Soon after addition of D_2O, the mixture was extracted with CH_2Cl_2 three times, and the combined organic layer was washed with brine. The organic layer was dried over $MgSO_4$ and removal of the solvent at room temperature under reduced pressure gave HCp*-d_1 as yellow oil. ^{1}H NMR ($CDCl_3$): δ 1.00 (s, 3H, Me), 1.76 (s, 6H, Me), 1.80 (s, 6H, 6-Me). MS (GC-EI): m/z = 137 ([M]$^+$).

Spin-Trapping Experiments. Spin-trapping experiments were performed with 2-methyl-2-nitrosopropane (MNP) dimer[41] or α-(4-pyridyl-*N*-oxide)-*N*-*tert*-butylnitrone (POBN)[41] as spin-trapping reagents to confirm the formation of carbon radicals in substrate oxidation reactions by $\mathbf{1}_{OX}$ and $\mathbf{2}_{OX}$. In the spin-trapping experiment with the MNP dimer, a solution of $\mathbf{1}_{OX}$ (11 μM) in CH_3CN was added to the solid of the MNP dimer (200 equiv) under Ar in the dark, and then indene (200 equiv) was added. This mixture was transferred into an ESR tube and the ESR spectrum was measured at room temperature under Ar. Spin-trapping experiments using POBN were conducted as follows: To a solution of $\mathbf{1}_{OX}$ or $\mathbf{2}_{OX}$ (11 μM) in MeCN, was added POBN (200 equiv). The solution was degassed to replace air to Ar and the mixture was cooled to −40 °C. Indene (100 equiv), fluorene (200 equiv), HCp* (200 equiv), or ethylbenzene (400 equiv) was added to the solution as a substrate and the mixture was incubated

DOI: 10.1021/jacs.6b03785
J. Am. Chem. Soc. 2016, 138, 9508–9520

for 30 min at −40 °C (the experiment using ethylbenzene was performed only with $\mathbf{1}_{OX}$, because $\mathbf{2}_{OX}$ cannot oxidize ethylbenzene under our conditions). This mixture was transferred into an ESR tube and the ESR spectra were measured at room temperature under Ar.

Single Crystal X-ray Diffraction Analyses of 2 and 2-H$^+$. Single crystals of **2** and (**2**-H$^+$)·(PF_6) were obtained by slow concentration of a CD_3CN solution of **2** and a $(CD_3)_2CO$ solution of (**2**-H$^+$)·(PF_6). All diffraction data were collected at 120 K on a Bruker APEXII diffractometer. The structures were solved by a direct method (SIR−97) and expanded with differential Fourier technique. All non-hydrogen atoms were refined anisotropically and the refinement was carried out with full matrix least-squares on *F*. All calculations were performed by using the Yadokari−XG software package.[42] Crystallographic data for **2** and (**2**-H$^+$)·(PF_6) are summarized in Table S1.

RESULTS

Synthesis of a Pterin Complex, 2. A novel Ru^{II}-pterin complex, [RuCl(Hdmdmp)(MeBPA)]$^+$ (**2**-H$^+$), was prepared simply by heating the solution of Hdmdmp and [$RuCl_3$(MeBPA)] in aqueous EtOH solution at reflux. Addition of an excess amount of Et_3N into the solution of **2**-H$^+$ afforded [Ru(dmdmp)Cl(MeBPA)] (**2**). However, as discussed below, the dmdmp ligand of **2** has strong basicity and tends to capture a proton from water or other impurities in the solution. Purification of **2** was performed by reprecipitation and repeated column chromatography on Sephadex LH20 eluted by MeOH to achieve thorough elimination of purplish fractions containing **2**-H$^+$. The careful purification resulted in relatively low yield of **2** (40%); however, crude **2** and relatively pure **2**-H$^+$ could be recovered from other fractions.

Crystal Structures of 2 and 2-H$^+$. From a CD_3CN solution of **2** and a $(CD_3)_2CO$ solution of **2**-H$^+$·PF_6, their single crystals suitable for X-ray crystallography were obtained by slow concentration of the solutions through vaporization of the solvents. The crystal structures of **2** and **2**-H$^+$ are shown in Figure 1a and 1b, respectively, with atom labeling. The geometries around the Ru^{II} ions of **2** and **2**-H$^+$ are octahedral with slight distortion. The bond lengths around the Ru centers fell in the normal range of those of Ru^{II} complexes. As described above, the pterin ligand of **2** can accept a proton relatively easily at one of the nitrogen atoms, and hence, the crystal structures of **2** and **2**-H$^+$ were distinguished based on the number of counteranions included in the crystal structure. The crystal of **2** contained no counterion, whereas the crystal of **2**-H$^+$ did one hexafluorophosphate ion (PF_6^-) per one Ru^{II}-pterin-MeBPA moiety. The deprotonated dmdmp$^-$ ligand has two possible resonance forms as shown in Scheme 2, *amidate* and *imidate* forms. The pterin ligand of **2** can be considered as in between the *imidate* form and the *amidate* one. The bond length of C2−O1 (1.273(6) Å) is longer than those of carbonyl C═O bonds (1.20−1.23 Å)[43] and shorter than those of phenolic C−O single bond (ca. 1.36 Å)[43] and the bond length of C2−N2 (1.343(9) Å) is shorter than those of C−N single bonds found in the MeBPA ligand (1.49−1.52 Å) and rather close to those found in the pyridine rings of MeBPA (1.34−1.36 Å). On the other hand, in the crystal structure of **2**-H$^+$, the N1 atom of a molecule and Cl1 atom of another molecule are close to each other, indicating hydrogen bonding between them (N1···Cl1: 3.285(2) Å) (Figure S1). Thus, it is clarified that the pterin ligand of **2**-H$^+$ in the crystal is protonated at the N1 atom (formally the 1-position in the pteridine skeleton).[44] The pterin ligand of **2**-H$^+$ was also recognized to be in between the *imidate* and the *amidate* forms as observed in **2**, on the basis of the bond lengths of C2−O1 (1.261(4) Å) and C2−N2 (1.340(3) Å). Thus, regardless of the protonation of the N1 nitrogen, the pterin ligands in **2** and **2**-H$^+$ are in the anion-delocalized form as shown in Scheme 2 (lower part).

Scheme 2. Two Resonance Forms and an Anion-Delocalized Form of Ru^{II}-dmdmp Complexes

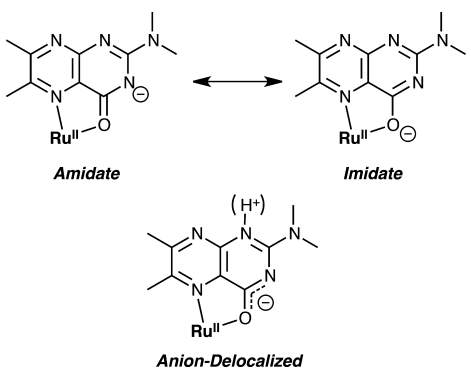

As a difference between the crystal structures of **2** and **2**-H$^+$, the bond length of Ru−N3 was barely elongated with protonation (Ru−N3 for **2**: 2.064(4) Å, Ru−N3 for **2**-H$^+$: 2.078(2) Å). This elongation should be derived from weakening of electron-donating ability of the pterin ligand due to the protonation, which causes the charge neutralization of the pterin ligand. In contrast, the Ru−Cl bond length was shortened with protonation (Ru−Cl for **2**: 2.437(2) Å, Ru−Cl for **2**-H$^+$: 2.4220(8) Å), because the electron donation from the pterin ligand to the Ru^{II} center should be reduced due to the protonation. To compensate the reduced electron density, the Ru^{II} center attracts the chloride ligand more strongly. In both crystal structures of **2** and **2**-H$^+$, steric hindrance was recognized between the pyridine ring containing N7 atom of the MeBPA ligand and the methyl group at the 6-position of the pterin ligand; as a result of the steric hindrance, the bond angles of N3−Ru−N7 became larger than 90° (∠N3−Ru−N7 for **2**: 106.3(2)°, ∠N3−Ru−N7 for **2**-H$^+$: 103.81(9)°). Although the two donating ligands (the π-donating chloride and σ-donating tertiary-amine ligands) bind at the *trans* positions to each other in **2** and **2**-H$^+$, the structures should be stabilized by intramolecular hydrogen bonding among the chloride ligand and the hydrogen atoms at the 6-positions of the pyridine rings of MeBPA. In the crystals of **2** and **2**-H$^+$, the distances between the chloride ligand and the carbon atoms at the 6-positions of the two pyridine rings in the MeBPA ligand are 3.372(6) Å and 3.345(7) Å for **2**, and 3.337(4) Å and 3.353(3) Å for **2**-H$^+$, respectively. The distances are in the normal range (3.3−3.7 Å) of those between chloride and carbon atoms having nonclassical hydrogen bonding.[45] The hydrogen bonding in **2** and **2**-H$^+$ can cause their greater thermodynamic stability compared to other possible isomers, having different coordination arrangements.

The lowest two ^{1}H NMR signals of **2** were upfield-shifted in accordance with protonation (**2**: 9.46 and 9.56, **2**-H$^+$: 9.37 and 9.53, and **2**-2H$^+$: 9.07 and 9.41 ppm) (Figure 2). These signals can be assigned to the hydrogen atoms at the 6-position of the pyridine rings of the MeBPA ligand. The upfield shifts by protonation can be explained by the existence of hydrogen bonding between the chloride ligand and the hydrogen atoms at the 6-position of the pyridine rings. The protonation at the pterin ligands should induce reduction of the electron density at the Ru^{II} center due to π-back-donation from the Ru^{II} center

DOI: 10.1021/jacs.6b03785
J. Am. Chem. Soc. 2016, 138, 9508−9520

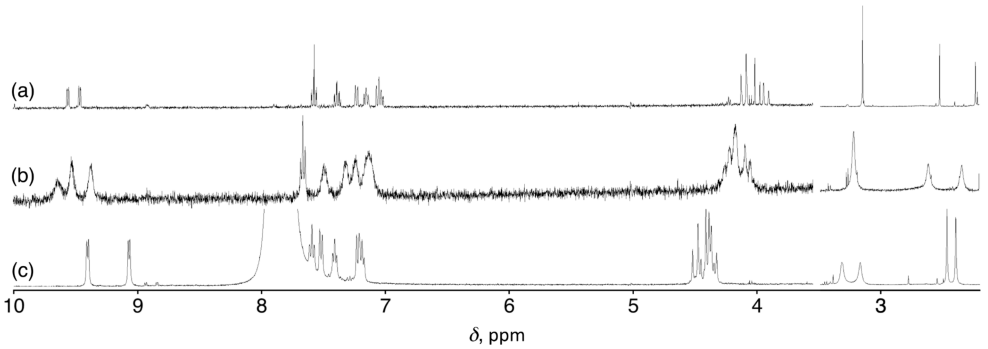

Figure 2. ^{1}H NMR spectra in CD_3CN of (a) **2** with K_2CO_3, (b) **2**-H$^+$ with $MgSO_4$, and (c) **2**-2H$^+$ with TfOH. The spectrum of **2**-2H$^+$ shows a large and broadened signal in the chemical shift range of 7.7−8.0 ppm derived from the large amount of the acid added to the solution.

to the π^*-orbitals of the pterin ligand, and the Ru^{II} center should attract the chloride ligand more strongly to compensate the reduction of the electron density, as reflected on the change of the Ru−Cl bond lengths (Ru−Cl for **2**: 2.437(2) Å, Ru−Cl for **2**-H$^+$: 2.4220(8) Å). The relatively electron-poor chloride ligands are expected to form weaker hydrogen bonds with the hydrogen atoms at the 6-positions than those in **2**, which probably cause the upfield shifts of the ^{1}H NMR signals upon protonation of **2** to form **2**-H$^+$ (Scheme 3).

Scheme 3. Effect of Protonation on the Chemical Shifts of the 6-H Protons of the MeBPA Ligand

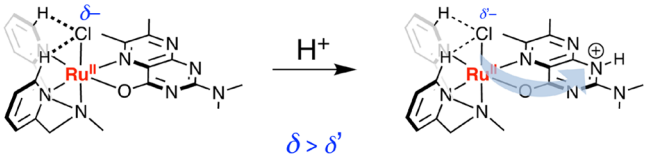

Evaluation of Basicity of 2 and 2-H$^+$: Determination of pK_a values of 2-H$^+$ and 2-2H$^+$. The pK_a value of **2**-H$^+$ in MeCN was determined by UV−vis titration with addition of 2,4,6-trimethylpyridine (Me_3Py, pK_a of Me_3Py-H$^+$ = 14.98)[46] as a base to an MeCN solution of **2**-H$^+$ prepared by addition of 1 equiv of trifluoromethanesulfonic acid (TfOH) into a solution of **2** (Figure 3a). In the course of the titration, the absorption spectrum of **2**-H$^+$ changed into that of **2** by addition of an excess amount of Me_3Py; that is, increase of absorbance at 392 and 495 nm and decrease of those at 326, 363, and 549 nm were observed with two isosbestic points at 373 and 519 nm, as shown in Figure 3a. The spectrum of **2** turned back to that of **2**-H$^+$ with addition of TfOH as an acid.

The pK_a value of the first protonation step to form **2**-H$^+$ was determined to be 16.4 on the basis of fitting analysis of the absorbance change at 430 nm (Figure S2a) and the pK_a value of Me_3Py-H$^+$. The UV−vis titration for further protonation of **2**-H$^+$ was performed using TfOH (pK_a = 2.60)[47] as one of the strongest proton donors in MeCN. The second protonation showed another spectral change with increase of absorbance at 300, 446, and 663 nm and simultaneous decrease of absorbance at 326, 363, and 549 nm, implying disappearance of **2**-H$^+$ (Figure 3b). Four isosbestic points were observed at 311, 412, 473, and 588 nm and reversibility of the change was also confirmed by addition of Et_3N. The pK_a value of the second protonation step of **2** to form the diprotonated form, **2**-2H$^+$, was determined to be 3.9, on the basis of fitting analysis of the

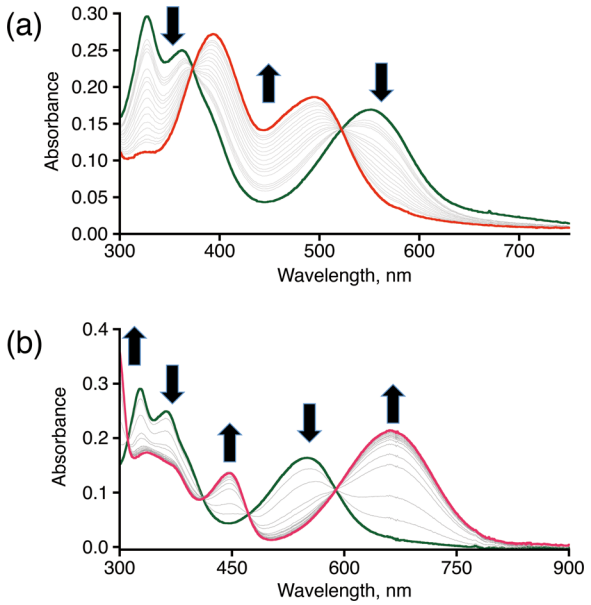

Figure 3. Absorption spectral changes in the course of base and acid titration of **2**-H$^+$ in MeCN at 296 K: (a) the deprotonation of **2**-H$^+$ (20.1 μM) upon addition of Me_3Py and (b) the protonation of **2**-H$^+$ (17.4 μM) upon addition of TfOH.

absorbance change at 549 nm (Figure S2b) and the pK_a value of TfOH.

The pK_a value of **1**-H$^+$ was reexamined in this work by using the same method for **2**-H$^+$ as mentioned above; the pK_a value of **1**-H$^+$ was determined to be 14.3 (Figure S2c and d).[48] The pK_a values of **1**-H$^+$ (14.3) and **1**-2H$^+$ (2.0)[34] are much smaller than those of **2**, indicating higher acidity of **1**-H$^+$ and **1**-2H$^+$ than that of **2**-H$^+$ and **2**-2H$^+$. Therefore, the dmdmp ligand in **2** has stronger basicity than that in **1**, reflecting larger electron density of the Ru^{II} center caused by ligand substitution from a π-accepting neutral ligand, pyridine, to a π-donating and anionic chloride ligand. Thus, it has been revealed that basicity of **2** is much larger than that of **1** in PCET reactions.

Electrochemical Measurements. Redox properties of **1**, **1**-H$^+$, and **1**-2H$^+$ in MeCN containing 0.1 M $TBAPF_6$ as an electrolyte were reported previously.[32d,33] Cyclic and differential-pulse voltammograms (CV and DPV) of **2**, **2**-H$^+$, and **2**-2H$^+$ were measured under the same conditions as the measurements for **1** and the protonated forms. All of **2**, **2**-H$^+$, and **2**-2H$^+$ showed one reversible oxidation waves at +0.24, +0.54, and +0.62 V vs SCE, respectively, which were assigned to the Ru^{II}/Ru^{III} processes (Figure S3). The large positive shift

DOI: 10.1021/jacs.6b03785
J. Am. Chem. Soc. 2016, 138, 9508−9520

of the Ru^{II}/Ru^{III} couple by the first protonation of the pterin ligand and the small positive shift by the second protonation were also observed in the measurements of **1** and the protonated forms (Table 1).[32d,33] In comparison of the redox

Table 1. Oxidation Potentials of the Ru-pterin Complexes in MeCN Containing 0.1 M $TBAPF_6$ as an Electrolyte

protonation status of pterin ligand	$E_{ox}(Ru^{II}/Ru^{III})$, V vs SCE (Fc/Fc$^+$)	
	1	**2**
dmdmp$^-$	+0.66 (+0.26)	+0.24 (−0.16)
Hdmdmp	+0.92 (+0.52)	+0.54 (+0.14)
H_2dmdmp$^+$	+0.94 (+0.54)	+0.62 (+0.22)

potentials of the corresponding protonated species between **1** and **2**, the redox potentials of **2** and the protonated forms are lower than those of **1** and the protonated forms, due to the ligand alteration of one π-accepting and neutral pyridine ring of the TPA ligand in **1** with the π-donating and negatively charged chloride ligand in **2**, together with the charges of the complex cations. Combined with effects of the ligand alteration on the pK_a values (14.3 for **1** and 16.4 for **2**) of the pterin ligand as mentioned above, the change of coordination environment and the charge of the complexes largely affected physical properties of the pterin complexes through change of electron density of the Ru^{II} centers.

The pK_a values and the first oxidation potentials of **2** and those of the protonated forms obtained in this work allowed us to draw "square schemes" of PCET reactions for **2** (Scheme 4b) and also to calculate BDEs based on eq 1, as in the case of

Scheme 4. Thermochemical Square Schemes for Multistep PCET of 1 (a) and 2 (b) in MeCN

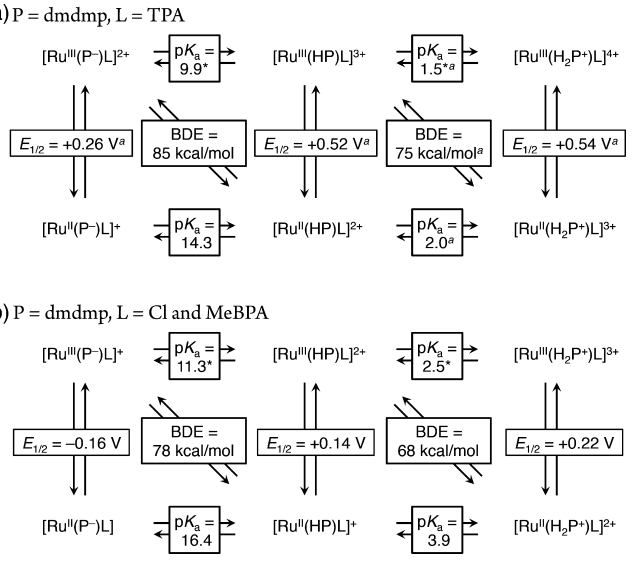

[a]Values taken from ref 34. *Calculated pK_a values on the basis of eq 1. $E_{1/2}$ values are referenced to ferrocene/ferrocenium.

1 (Scheme 4a).[16−19] In the case of MeCN as a solvent, the *C* value in eq 1 is estimated to be 59.5 kcal mol^{-1} with use of redox potentials against the ferrocene/ferrocenium couple.[15] Also in our calculations, the potentials vs SCE are converted to the values against ferrocene/ferrocenium couple by subtraction of 0.40 V (see Table 1).[34] In this study, we adopted BDE rather than bond dissociation free-energy (BDFE),[39,49] because small contribution of the entropy term should be expected.[49,50] The BDE values for the H atom abstraction reaction from **2**-H$^+$ to give $[Ru^{III}(dmdmp)Cl(MeBPA)]^+$ ($\mathbf{2}_{OX}$) was calculated to be 78 kcal mol^{-1}, and that for the reaction from **2**-2H$^+$ to give $[Ru^{III}Cl(Hdmdmp)(MeBPA)]^{2+}$ ($\mathbf{2}_{OX}$-H$^+$) was determined to be 68 kcal mol^{-1}: The BDE values for **2**-H$^+$ and **2**-2H$^+$ are lower than those for the corresponding **1**-H$^+$ and **1**-2H$^+$ (85 and 75 kcal mol^{-1}).[51] Thus, $\mathbf{2}_{OX}$ is expected to show thermodynamically lower reactivity in CPET reactions than $\mathbf{1}_{OX}$.

H Atom Transfer from C−H Bonds of Organic Substrates to $\mathbf{1}_{OX}$ and $\mathbf{2}_{OX}$. Complexes **1** and **2** were oxidized with addition of 1 equiv of $[Fe^{III}(bpy)_3]^{3+}$ (E_{red} = +1.10 V vs SCE)[52] as an oxidant in MeCN in accordance with the procedure described in our previous report.[34] The absorption spectrum of **1** and **2** in MeCN exhibited the absorption maxima at 407 and 461 nm for **1** and 392 and 493 nm for **2** as the red trace (Figure 4). Upon addition of the

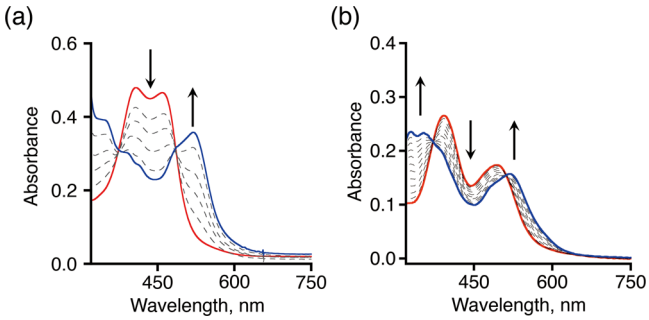

Figure 4. UV−vis spectral changes in the course of the titration of $[Fe^{III}(bpy)_3](PF_6)_3$ as a 1e$^-$-oxidant into the solution of **1** (a) and **2** (b) in MeCN at room temperature. Red trace: 0 equiv. Blue trace: 1 equiv.

oxidant in the MeCN solution of **1** and **2**, the corresponding spectra changed with two isosbestic points at 373 and 486 nm for **1** and 372 and 510 nm for **2** as depicted in Figure 4.

In the course of the reaction, the increase of absorbance at 520 nm was observed due to the formation of $[Fe^{II}(bpy)_3]^{2+}$. The absorption spectrum of the 1e$^-$-oxidized form of **2**, $\mathbf{2}_{OX}$, was obtained by subtraction of the spectrum of $[Fe^{II}(bpy)_3]^{2+}$ from the final spectrum (blue line). The spectrum of $\mathbf{2}_{OX}$ exhibited the absorption maxima at 366 and 517 nm (Figure S4b). In addition, the absorption spectrum of the 1e$^-$-oxidized form of **1**, $\mathbf{1}_{OX}$, was similarly obtained by subtraction of the spectrum of $[Fe^{II}(bpy)_3]^{2+}$, as shown in Figure S4a.

The 1e$^-$-oxidized species of **1** and **2** ($\mathbf{1}_{OX}$ and $\mathbf{2}_{OX}$, respectively) reacted with substrates such as hydrocarbons in MeCN (Table 2). The oxidation reactions of organic substrates with $\mathbf{1}_{OX}$ and $\mathbf{2}_{OX}$ were monitored on a stopped-flow apparatus in a double-mixing mode. In the reaction of $\mathbf{1}_{OX}$ with 9,10-dihydroanthracene (DHA) as a substrate, the absorbance at 497 nm, which was assigned to that of **1**-H$^+$,[34] increased as demonstrated in Figure 5a. In the case of the reaction of $\mathbf{2}_{OX}$ with DHA, the absorbance at 528 nm due to **2**-H$^+$ increased as shown in Figure 5b. The spectral changes indicate the formation of **1**-H$^+$ or **2**-H$^+$ in the course of the reaction of $\mathbf{1}_{OX}$ or $\mathbf{2}_{OX}$ with DHA. In both cases, characteristic absorption bands of anthracene as the product increased in the range of λ < 400 nm with vibronic features (ε = 7.2 × 10^3 M^{-1} cm^{-1} at 374 nm)[26a] (Figure 5).[53] To clarify the final products derived

DOI: 10.1021/jacs.6b03785
J. Am. Chem. Soc. 2016, 138, 9508−9520

Table 2. Oxidation Potentials, pK_a and BDE Values of Hydrocarbons, and Second-Order Rate Constants of C−H Oxidation Reactions by $\mathbf{1}_{OX}$ or $\mathbf{2}_{OX}$ in MeCN at 296 K

substrate	E_{ox}, V vs SCE	pK_a	BDE, kcal mol^{-1}	k, M^{-1} s^{-1}	
				$\mathbf{1}_{OX}$	$\mathbf{2}_{OX}$
HCp*	+0.95[a]	37.1[b]	77[c]	(6.0 ± 0.2) × 10^4	(5.7 ± 0.2) × 10^2
xanthene	+1.56[a]	41.0[b]	76[c]	(1.3 ± 0.1) × 10^3	(8.7 ± 0.4) × 10^2
DHA	+2.13[a]	41.1[b]	76[c]	(2.5 ± 0.1) × 10^2	87 ± 2
fluorene	+1.58[a]	33.6[b]	82[c]	36 ± 1	1.4 ± 0.1
indene	+1.54[a]	31.1[b]	83[c]	13 ± 1	0.24 ± 0.01
ethylbenzene	+2.41[a]	–	85[c]	0.50 ± 0.02	too slow

[a]Determined by second-harmonic alternating current voltammetry (SHACV) in MeCN. [b]Values measured in DMSO (ref 55) and extrapolated to those in MeCN using the equation: p$K_{a(C-H)}$ (in CH_3CN) = 11 + p$K_{a(C-H)}$ (in DMSO) (ref 17). [c]ref 56.

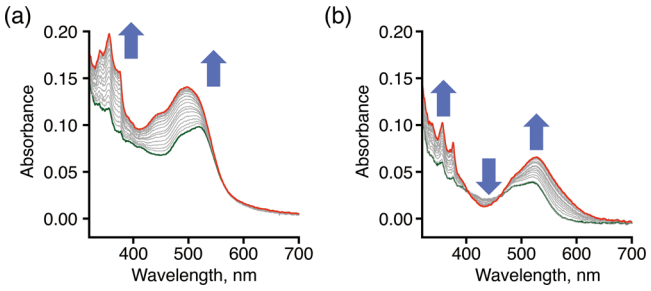

Figure 5. Absorption spectral changes in the course of the reactions of 9,10-dihydroanthracene (DHA) with $\mathbf{1}_{OX}$ (a) and $\mathbf{2}_{OX}$ (b) monitored by a stopped-flow spectrometer in MeCN at 296 K: [Ru] = 15 μM, [DHA] = 2.4 mM. Green trace: 0 s. Red trace: 9.9 s.

from $\mathbf{1}_{OX}$ and $\mathbf{2}_{OX}$ in the DHA oxidation, the differential spectra were obtained by the subtraction of the spectrum of $[Fe(bpy)_3]^{2+}$ (15 μM in MeCN) from the final spectra of the reaction mixtures (Figure 6). The spectra of the products from

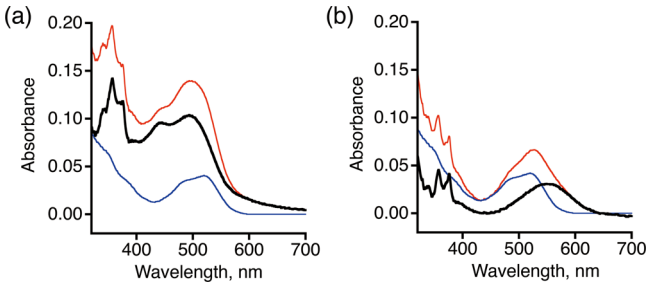

Figure 6. Differential spectra obtained for the reactions of DHA with $\mathbf{1}_{OX}$ (a) and $\mathbf{2}_{OX}$ (b) in MeCN: The final spectra of the reactions are described with red traces, those of $[Fe^{II}(bpy)_3]^{2+}$ (15 μM) are with blue traces, and those obtained by (red) − (blue) are with black traces.

the oxidants, shown as the black traces in Figure 6, are identical to the spectrum of $\mathbf{1}$-H$^+$ as represented by the absorptions at 443 and 493 nm[54] and that of $\mathbf{2}$-H$^+$ as supported by the absorption at 549 nm, which is consistent with the green line in Figure 3b, respectively. Thus, it is concluded that a proton and an electron of a C−H bond of DHA are transferred to the N-1 position of the dmdmp$^-$ ligand and to the Ru^{III} center, respectively, through a PCET mechanism as shown in Scheme 5. In addition, the ESR spectral changes in the reactions of $\mathbf{1}_{OX}$ and $\mathbf{2}_{OX}$ with xanthene also suggested that complexes $\mathbf{1}_{OX}$ and $\mathbf{2}_{OX}$ were reduced from the Ru^{III} to Ru^{II} states in the course of the oxidation reactions (Figure S5).

Product analyses were conducted for the oxidation reactions of the respective substrates. According to the UV−vis spectral changes, the oxidation of DHA gave anthracene as mentioned above. In the oxidation of xanthene with $\mathbf{1}_{OX}$ at high concentration, formation of xanthylium cation[57] was suggested by absorption at 370 nm (Figure S6). Attempts to detect the products of the oxidation reactions of other substrates were performed using GC-MS; however, no signals of organic products were detected. The indenyl radical, which is presumed to be formed from the oxidation of indene with $\mathbf{1}_{OX}$ and $\mathbf{2}_{OX}$, has been known to polymerize rapidly;[58] hence, the indenyl radical formed probably should further react rapidly to afford polymers, which are insensitive to the GC measurements. Supporting this, in SHACV measurements of an indene solution in MeCN, the working electrode of glassy carbon disk was coated with brown materials, which were assumed to be indenyl polymers. Therefore, to confirm the formation of the indenyl radical, the detection of the ESR signal of a spin adduct was performed using 2-methyl-2-nitrosopropane (MNP) dimer as a spin trapping reagent.[59] A solution of $\mathbf{1}_{OX}$ in CH_3CN (11 μM) was added to the solid of MNP dimer (200 equiv) in the dark, and then indene (200 equiv) was added. Right after the addition, ESR spectrum of the reaction mixture was measured at room temperature. As a result, a triplet of doublets (g = 2.0064, A_N = 14.7 G, A_H = 2.4 G) was observed as shown in Figure S7a, which was assigned to a nitroso radical coupled with one hydrogen atom obtained by

Scheme 5. Reactions of $\mathbf{2}_{OX}$ with Substrates

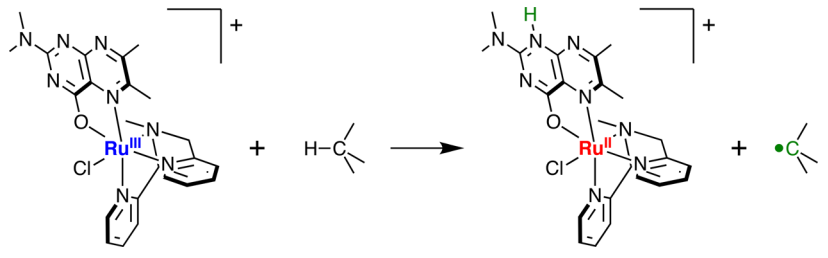

DOI: 10.1021/jacs.6b03785
J. Am. Chem. Soc. 2016, 138, 9508−9520

adduct formation between MNP and indenyl radical.[41] Control experiments indicate that the short-lived indenyl radical should be formed in the reaction of indene with $\mathbf{1}_{OX}$, and the ESR signal is derived from neither self-decomposition of MNP dimer (Figure S7g) nor oxidation reactions of indene by $[Fe^{III}(bpy)_3]^{3+}$ (Figure S7d).

The aforementioned electrode-coating phenomena was also observed in the electrochemical measurements of an HCp* solution in MeCN; thus, oxidized HCp* is also assumed to form polymers. C−H abstraction from fluorene at the 9-position has been reported to afford 9*H*,9′*H*-[9,9′]bifluorenyl as a product;[60] however, we could not detect any dimeric products. Thus, we performed spin-trapping ESR measurements using α-(4-pyridyl-*N*-oxide)-*N*-*tert*-butylnitrone (POBN)[61] to support the formation of indenyl, fluorenyl, pentamethylcyclopentadienyl, and ethylbenzyl radicals as products of PCET oxidation of indene, fluorene, HCp*, and ethylbenzene, respectively, by $\mathbf{1}_{OX}$ or $\mathbf{2}_{OX}$. To the solution of $\mathbf{1}_{OX}$ or $\mathbf{2}_{OX}$ (11 μM) in MeCN was added POBN (200 equiv), and then, the atmosphere was replaced with Ar and the mixture was cooled to −40 °C. An excess amount of one of the substrates was added to the solution and the mixture was incubated for 30 min at −40 °C. The ESR spectrum of the solution was measured at room temperature. We could observe a triplet of doublets derived from a spin adduct of POBN with a carbon-centered radical as an oxidation product for all of the four substrates (Figure S8 and S9).

Kinetics of C−H Oxidation with $\mathbf{1}_{OX}$ and $\mathbf{2}_{OX}$. The absorbance change of the solution containing $\mathbf{2}_{OX}$ at 530 nm obeyed pseudo-first-order kinetics in the presence of an excess amount of DHA as shown in Figure 7a and curve-fitting of the

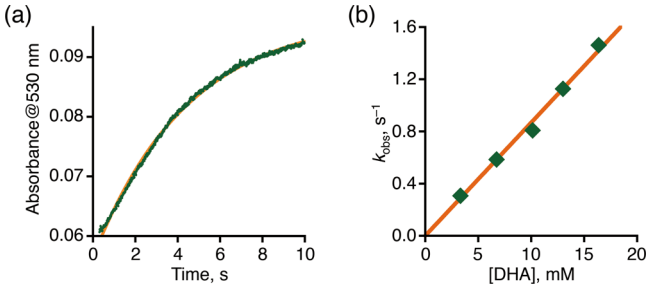

Figure 7. (a) The change of absorbance at 530 nm (green dot) and the pseudo-first-order fitting curve (orange line) in the course of the reaction of $\mathbf{2}_{OX}$ with DHA monitored by a stopped-flow spectrometer in MeCN at 296 K: [Ru] = 15 μM, [DHA] = 3.3 mM. (b) Concentration dependence of k_{obs} for the reaction between $\mathbf{2}_{OX}$ and DHA (green filled squares) and the curve fitting analysis (orange solid line).

time-course of the absorbance at 530 nm allowed us to determine a pseudo-first-order rate constant (k_{obs}). On the basis of a plot of the k_{obs} values versus the concentrations of the substrate (Figure 7b), we determined the second-order rate constants (k) from the slope of the linear correlation as depicted in Figure 7b. The k values of the DHA oxidation by $\mathbf{1}_{OX}$ and $\mathbf{2}_{OX}$ were determined to be $(2.5 \pm 0.1) \times 10^2$ M^{-1} s^{-1} and 87 ± 2 M^{-1} s^{-1}, respectively. A Ru^{IV}=O complex, $[Ru^{IV}(O)(bpy)_2(py)]^{2+}$, which has a similar BDE value (85 kcal mol^{-1}) to those of $\mathbf{1}_{OX}$ and $\mathbf{2}_{OX}$, has been reported to oxidize DHA with the rate constant of $k = 1.25 \times 10^2$ M^{-1} s^{-1}.[62] Thus, the rate constants of $\mathbf{1}_{OX}$ and $\mathbf{2}_{OX}$ for the DHA oxidation are comparable to that of Ru^{IV}=O complexes with similar driving forces in light of the BDE values.

In accordance with this procedure, the k values for C−H oxidation reactions of a series of substrates were determined in MeCN at 296 K (Figures S10−S15). The second-order rate constants for oxidation reactions of other substrates by $\mathbf{1}_{OX}$ and $\mathbf{2}_{OX}$ are summarized in Table 2. Complexes $\mathbf{1}_{OX}$ and $\mathbf{2}_{OX}$ showed similar reactivity in the oxidation reaction of xanthene, with comparable rate constants ($(1.3 \pm 0.1) \times 10^3$ M^{-1} s^{-1} for $\mathbf{1}_{OX}$, $(8.7 \pm 0.4) \times 10^2$ M^{-1} s^{-1} for $\mathbf{2}_{OX}$). In contrast, for the C−H oxidation of other substrates, the reactivity of the two complexes were different; for example, the k value for the reaction of 1,2,3,4,5-pentamethyl-cyclopentadiene (HCp*) with $\mathbf{1}_{OX}$ was ca. 100 times larger than that with $\mathbf{2}_{OX}$: k = $(6.0 \pm 0.2) \times 10^4$ M^{-1} s^{-1} for $\mathbf{1}_{OX}$ and $(5.7 \pm 0.2) \times 10^2$ M^{-1} s^{-1} for $\mathbf{2}_{OX}$. In addition, the k values in the indene oxidation were 13 ± 1 M^{-1} s^{-1} for $\mathbf{1}_{OX}$ and 0.24 ± 0.01 M^{-1} s^{-1} for $\mathbf{2}_{OX}$, respectively. As for ethylbenzene (BDE_{C-H} = 85.4 kcal mol^{-1}), $\mathbf{1}_{OX}$, showing the BDE value of 85 kcal mol^{-1}, reacted slowly with the substrate at the rate constant of 0.50 ± 0.02 M^{-1} s^{-1}; however, the reaction of $\mathbf{2}_{OX}$, showing the BDE value of 78 kcal mol^{-1}, with ethylbenzene did not proceed, because of the energetically uphill situation in light of the BDE values of the oxidant and the substrate. This result is consistent with the relationship of the BDE values of both complexes and the substrates, indicating that the C−H oxidation by $\mathbf{1}_{OX}$ and $\mathbf{2}_{OX}$ proceed through a CPET mechanism (see below). The activation parameters were determined from kinetic analysis using the Eyring plots for oxidation reactions of indene, DHA, xanthene, HCp*, and fluorene with $\mathbf{1}_{OX}$ and $\mathbf{2}_{OX}$ (Figures 8, S16 and Table 3).[63]

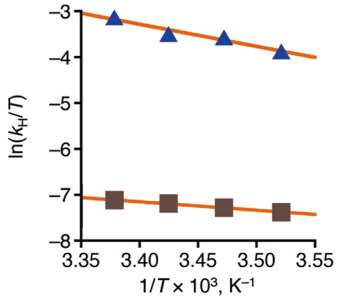

Figure 8. Eyring plots for the oxidation of DHA by $\mathbf{1}_{OX}$ (blue triangles) and $\mathbf{2}_{OX}$ (brown squares) in MeCN.

To elucidate the C−H bond cleavage process, kinetic isotope effects (KIE) were also investigated for the oxidation reactions of HCp* (HCp* and DCp*), DHA (DHA and DHA-d_4) with $\mathbf{1}_{OX}$ or $\mathbf{2}_{OX}$ (Figure S13 and S14), and KIE for the oxidation

Table 3. Activation Parameters for Oxidation of C−H Bonds with $\mathbf{1}_{OX}$ and $\mathbf{2}_{OX}$

	$\mathbf{1}_{OX}$		$\mathbf{2}_{OX}$	
substrates	$\Delta S^{\ddagger a}$	$\Delta H^{\ddagger b}$	$\Delta S^{\ddagger a}$	$\Delta H^{\ddagger b}$
indene	−21 ± 5	9 ± 2	−49 ± 1	3.6 ± 0.1
DHA	−28 ± 1	5.6 ± 0.3	−33 ± 3	4.8 ± 0.8
xanthene	−21 ± 2	6.9 ± 0.7	−32 ± 2	4.0 ± 0.6
HCp*	−22 ± 1	4.5 ± 0.7	−17 ± 5	9 ± 1
fluorene	−45 ± 1	1.9 ± 0.2	−51 ± 1	2.0 ± 0.1

[a]cal K^{-1} mol^{-1}. [b]kcal mol^{-1}.

DOI: 10.1021/jacs.6b03785
J. Am. Chem. Soc. 2016, 138, 9508−9520

reaction of ethylbenzene (ethylbenzene and ethylbenzene-d_{10}) with $\mathbf{1}_{OX}$ was examined (Figure S15). In the oxidation of DHA, both $\mathbf{1}_{OX}$ and $\mathbf{2}_{OX}$ showed relatively large KIE values (k_H/k_D): 4.2 ± 0.3 for $\mathbf{1}_{OX}$ and 4.5 ± 0.2 for $\mathbf{2}_{OX}$. For the oxidations of ethylbenzene with $\mathbf{1}_{OX}$ and HCp* by $\mathbf{2}_{OX}$, KIE values were determined to be 1.67 ± 0.08 and 8.1 ± 0.4, respectively. In stark contrast, the oxidation reaction of HCp* with $\mathbf{1}_{OX}$ gave a small KIE value of 1.33 ± 0.06.

DISCUSSION

The normal KIE values, observed for oxidations of DHA and ethylbenzene by $\mathbf{1}_{OX}$ and DHA and HCp* by $\mathbf{2}_{OX}$ (see above), indicate that the reactions involve hydrogen-atom abstraction process as the rate-determining step, and thus, the C−H oxidations proceed through a CPET mechanism rather than a stepwise PT/ET or ET/PT mechanism. C−H oxidation reactions by nonporphyrin metal-oxo complexes including Ru^{IV}=O complexes have been reported to exhibit large k_H/k_D values (18−50) in the kinetic isotope-labeling experiments;[62,64] for example, the k_H/k_D value of the DHA and DHA-d_4 oxidation by $[Ru^{IV}(O)(bpy)_2(py)]^{2+}$ was reported to be 35 ± 1.[62] On the other hand, the k_H/k_D values of the DHA and DHA-d_4 oxidation by $\mathbf{1}_{OX}$ and $\mathbf{2}_{OX}$ were determined to be 4.2 ± 0.3 and 4.5 ± 0.2, respectively (see above). The BDE values of the oxidants, $[Ru^{IV}(O)(bpy)_2(py)]^{2+}$ (85 kcal mol^{-1}), $\mathbf{1}_{OX}$ (85 kcal mol^{-1}), and $\mathbf{2}_{OX}$ (78 kcal mol^{-1}) are very similar, and the rate constants of the DHA oxidation at 296 K are also comparable. The very large KIE value indicates that the C−H oxidation by the Ru^{IV}=O complex proceeds through a tunneling mechanism.[62] On the contrary, in light of the smaller KIE values, the C−H oxidation by $\mathbf{1}_{OX}$ and $\mathbf{2}_{OX}$ proceeds via a mechanism involving a certain potential barrier without tunneling.

On the basis of the small KIE value (1.33 ± 0.06) for the oxidation reaction of HCp* with $\mathbf{1}_{OX}$, the reaction is proposed to proceed through an ET/PT mechanism rather than a CPET pathway. To confirm this proposal, we examined oxidation of HCp* by $\mathbf{1}_{OX}$ with use of large excess HCp* to enhance the first ET step. Just after mixing large excess HCp* (18 mM) and $\mathbf{1}_{OX}$ (16 μM) solutions (at 0 ms in Figure S17a) at 296 K, we could observe an absorption band around 400 nm due to the 1e$^-$-oxidized HCp* ($HCp^{*\bullet+}$; Figure S17b). This result clearly indicates that ET from HCp* to $\mathbf{1}_{OX}$ occurs prior to the subsequent PT from $HCp^{*\bullet+}$ to $\mathbf{1}$ ($[Ru^{II}(dmdmp)(TPA)]^+$) to afford $\mathbf{1}$-H$^+$ (Figure S17c). Thus, we have verified the stepwise ET/PT mechanism for the oxidation of HCp* by $\mathbf{1}_{OX}$ by the observation of 1e$^-$-oxidized HCp*, $HCp^{*\bullet+}$.[65] The lower E_{ox} value of HCp* (+0.95 V vs SCE), as compared to those of other substrates (+1.5−2.0 V vs SCE), probably enables the ET/PT mechanism with increasing the driving force of electron transfer ($-\Delta G_{ET}$) from HCp* to $\mathbf{1}_{OX}$ (+0.66 V vs SCE; see Table 1) to be −0.29 eV. Although the ET reaction is assumed to be energetically uphill, it could occur due to the Gibbs-energy gain from subsequent reactions to form a stable product, such as a polymer.[65]

Plots of log k' ($k' = k/n$; n = number of equivalent hydrogen atoms to be abstracted) for C−H oxidations with $\mathbf{1}_{OX}$ and $\mathbf{2}_{OX}$ against BDE values of the C−H bonds to be cleaved were prepared to argue the difference of the mechanisms, depending on the substrates and the oxidants (Figure 9). In the case of $\mathbf{1}_{OX}$, a much higher k' value was obtained for the oxidation of HCp* than those for other five substrates (see above). Except HCp*, the log k' values for the other four substrates showed a linear relationship relative to the BDE values of the C−H bonds, as depicted in Figure 9a. In the case of $\mathbf{2}_{OX}$, in contrast to the case of $\mathbf{1}_{OX}$, the log k' values for the oxidation reactions of the five hydrocarbons showed a linear relationship, without exception, with respect to the BDE values as depicted in Figure 9b. The linear correlations observed for the oxidation reactions by $\mathbf{1}_{OX}$ and $\mathbf{2}_{OX}$ indicate that the reactions proceed through a common mechanism for each complex. Thus, the oxidation of HCp* by $\mathbf{1}_{OX}$ is concluded to proceed in a different mechanism, i.e., an ET/PT mechanism, as mentioned above.

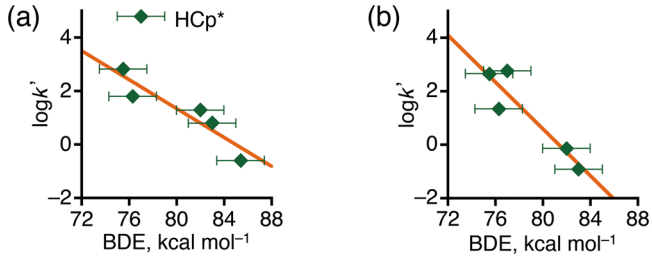

Figure 9. Plots of the log k' values at 296 K for oxidation of six hydrocarbon substrates with $\mathbf{1}_{OX}$ (a) and five hydrocarbon substrates with $\mathbf{2}_{OX}$ (b) against BDE values of C−H bonds to be cleaved in the substrates. In the linear fitting for (a), the k' value for oxidation of HCp* is not included for the calculations.

In general, the linear relationship between the second-order rate-constants and the BDE values of the C−H bonds to be cleaved has been analyzed on the basis of the Bell−Evans−Polanyi (BEP) relation as expressed by the following equations, 4 and 5:[66,67]

$$E_a = \alpha \Delta H^\circ + C \quad (4)$$

$$\Delta H^\circ = \mathrm{BDE}_{\mathrm{C-H\ to\ be\ cleaved}} - \mathrm{BDE}_{\mathrm{oxidant}} \quad (5)$$

Logarithm of rate constants of C−H oxidation reactions by high-valent metal-oxo complexes, which are excellent oxidants to oxidize organic substrates, generally obey the BEP relation to give coefficients of $\alpha \sim -0.5$.[62] In the case of a metal complex having a hydroxo ligand as a basic site as an oxidant in HAT, the α values have been reported by Stack and co-workers to be −0.1 (Mn^{III}−OH)[68] and −0.2 (Fe^{III}−OH),[69] which are smaller than those with metal-oxo complexes as oxidants. Except the oxidation of HCp* by $\mathbf{1}_{OX}$, the log k' values for oxidation reactions of hydrocarbons with $\mathbf{1}_{OX}$ and $\mathbf{2}_{OX}$ obeyed the BEP correlation and the coefficients α were determined to be −0.27 for $\mathbf{1}_{OX}$[70] in Figure 9a and −0.44 for $\mathbf{2}_{OX}$ in Figure 9b, respectively. The difference between the α values for $\mathbf{1}_{OX}$ and $\mathbf{2}_{OX}$ highlights distinguishable alteration of characteristics of transition states in the PCET reactions of C−H bonds by both oxidants.

Leffler advocated that the coefficient α of the BEP correlations reflected the structure of the transition state;[71] based on the discussion, a reaction passing through the transition state with the structure reminiscent of that of the product show a larger negative α value, whereas that passing through the transition state with the structure reminiscent of that of the starting material affords a smaller absolute value of α.[62,69] From this viewpoint, the coefficient α of the oxidation reactions with $\mathbf{1}_{OX}$ suggest that the reaction proceeds via a transition state involving a structure close to the initial structure, as compared to that of the oxidation by $\mathbf{2}_{OX}$: The proton to be transferred should interact strongly with the attached carbon atom of a substrate. On the contrary, the

DOI: 10.1021/jacs.6b03785
J. Am. Chem. Soc. 2016, 138, 9508−9520

reactions by $\mathbf{2}_{OX}$ go through a transition state involving a structure relatively close to the product as compared to the case of $\mathbf{1}_{OX}$ and the proton should interact more strongly with the N1 atom of the dmdmp$^-$ ligand than in the reaction with $\mathbf{1}_{OX}$.

The arguments on the difference in the transition states can be supported by the difference of characteristics of the two complexes, in light of the redox potentials of the Ru^{II}/Ru^{III} couples (+0.66 V for $\mathbf{1}_{OX}$ and +0.24 V for $\mathbf{2}_{OX}$; see Table 1 and Scheme 4), representing the electron-acceptability at the Ru^{III} center, and the pK_a values of the Ru^{III}-bound dmdmp$^-$ ligand (9.9 for $\mathbf{1}_{OX}$ and 11.3 for $\mathbf{2}_{OX}$; see Scheme 4), standing for the basicity. Thus, complex $\mathbf{1}_{OX}$ has higher electron-acceptability and lower basicity, whereas $\mathbf{2}_{OX}$ has lower electron-acceptability and higher basicity. Thus, more basic $\mathbf{2}_{OX}$ pulls a proton from the substrate to be abstracted at the early stage of the HAT reaction based on its high basicity; the attractive interaction can cause large polarization of the C−H bond to compensate its low electron-acceptability (Scheme 6). The "proton-pulling"

Scheme 6. Proposed Arrangements of the Transition States in C−H Oxidation by $\mathbf{1}_{OX}$ and $\mathbf{2}_{OX}$

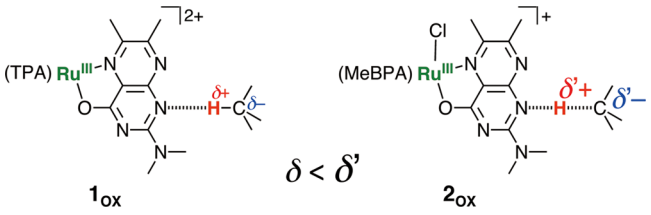

arrangement in the transition state induces the rise of electron acceptability of the Ru^{III} center and lowering of the oxidation potential of the substrate to be oxidized. On the other hand, since complex $\mathbf{1}_{OX}$ shows the higher electron-acceptability, even though complex $\mathbf{1}_{OX}$ shows lower basicity reflected on the higher redox potential, the complex requires not so much proton shift toward the dmdmp$^-$ ligand to gain large polarization of the C−H bond. Thus, we conclude that the polarization of the C−H bond in the transition state can be controlled by the basicity of the proton acceptor site as a prologue toward CPET, even though the apparent BDE values are comparable, and this causes the difference of the arrangement of the transition state in the C−H oxidation.

To shed further light on the difference in the transition states (TSs) of C−H oxidation by $\mathbf{1}_{OX}$ and $\mathbf{2}_{OX}$, DFT calculations were performed on the TSs of the oxidation reactions of indene with $\mathbf{1}_{OX}$ and $\mathbf{2}_{OX}$ (Figure 10). In the TS of the oxidation of indene by $\mathbf{1}_{OX}$, a hydrogen atom of the methylene moiety of the indene molecule interacts with the N1 of the pterin ligand of $\mathbf{1}_{OX}$ and the indene molecule rather resembles to its initial structure; a C−H bond of the methylene moiety of the indene molecule to be cleaved is 1.29 Å and the N1···H distance is 1.46 Å (Figure 10a). On the other hand, a hydrogen atom of the methylene moiety of the indene molecule is strongly attracted by N1 of the pterin ligand of $\mathbf{2}_{OX}$ in the TS and the C−H bond is elongated (1.34 Å) and the N···H distance is shortened to be 1.37 Å (Figure 10b). Therefore, we conclude that our assumption on the TS in the H atom abstraction by $\mathbf{1}_{OX}$ and $\mathbf{2}_{OX}$ based on the α value of the BEP plot is supported by the DFT calculations.

Apart from oxidation of HCp*, complex $\mathbf{2}_{OX}$ shows larger negative values of $\Delta S^{\ddagger}$ and smaller $\Delta H^{\ddagger}$ values than those of $\mathbf{1}_{OX}$ (Table 3). The larger $\Delta S^{\ddagger}$ values of $\mathbf{2}_{OX}$ are consistent with

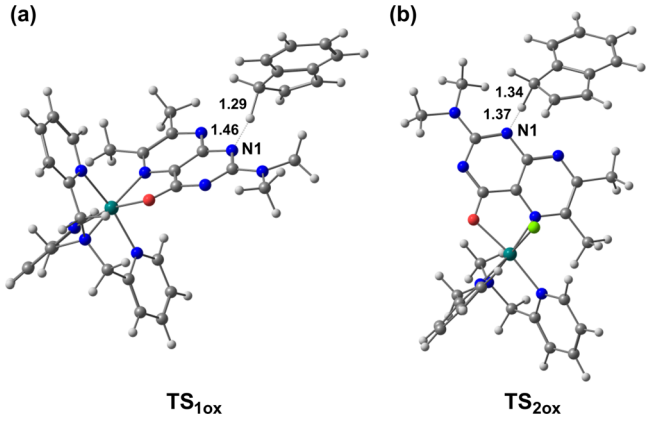

Figure 10. DFT-calculated transition states of the oxidation reactions of indene with $\mathbf{1}_{OX}$ (a) and $\mathbf{2}_{OX}$ (b).

the aforementioned proposal about the transition states; $\mathbf{2}_{OX}$ preforms oxidation reactions through more strongly interacted transition states than that of $\mathbf{1}_{OX}$. The smaller $\Delta H^{\ddagger}$ values of $\mathbf{2}_{OX}$ also correspond to difference between $\mathbf{1}_{OX}$ and $\mathbf{2}_{OX}$; $\mathbf{2}_{OX}$ is expected to have higher basicity (calcd. pK_a = 11.3) than that of $\mathbf{1}_{OX}$ (calcd. pK_a = 9.9) and the higher basicity must provide stable formation of the complex between the C−H bond to be cleaved and the dmdmp ligand of the oxidants in the transition state due to the larger polarization. In oxidation of HCp* with $\mathbf{1}_{OX}$ and $\mathbf{2}_{OX}$, the opposite tendency was observed in values of $\Delta S^{\ddagger}$ and $\Delta H^{\ddagger}$; $\mathbf{1}_{OX}$ shows larger negative (or comparable) values of $\Delta S^{\ddagger}$ and smaller $\Delta H^{\ddagger}$ values than those of $\mathbf{2}_{OX}$. The deviation from the tendency can be explained by the aforementioned proposal that complex $\mathbf{1}_{OX}$ oxidized HCp* through a different process (ET/PT) from that by $\mathbf{2}_{OX}$ (CPET). This large $\Delta S^{\ddagger}$ in the oxidation reaction of HCp* with $\mathbf{1}_{OX}$ can be attributed to the character of its transition state and the solvation. Among the oxidation reactions studied here, only that of HCp* with $\mathbf{1}_{OX}$ afforded radical cation species (HCp*$^{\bullet+}$) by ET instead of a neutral radical (Cp*$^{\bullet}$) by HAT. In outer-sphere electron transfer, reorganization of solvent molecules mainly controls the activation entropy of the reaction.[72−74] MeCN employed as the solvent in this study is expected to firmly solvate the molecules in the transition state in the ET reaction from HCp* to $\mathbf{1}_{OX}$, and the strong solvation probably derives the relatively large $\Delta S^{\ddagger}$.

From the $\Delta H^{\ddagger}$ and $\Delta S^{\ddagger}$ values, $\Delta G^{\ddagger}$ values for the C−H oxidation of hydrocarbons as the substrates can be determined. At 298 K, the differences between $\mathbf{1}_{OX}$ and $\mathbf{2}_{OX}$ in the $\Delta G^{\ddagger}$ values ($\Delta\Delta G^{\ddagger}$: $\Delta\Delta G^{\ddagger} = \Delta G^{\ddagger}(\mathbf{2}_{OX}) - \Delta G^{\ddagger}(\mathbf{1}_{OX})$) for oxidation of hydrocarbons are positive, indicating that higher activity of $\mathbf{1}_{OX}$ as an oxidant than that of $\mathbf{2}_{OX}$. Plot of the $\Delta\Delta G^{\ddagger}$ values showed linear relationship against BDE values of the C−H bonds to be cleaved except HCp* (Figure 11), which is oxidized though a different mechanism, i.e., ET/PT for $\mathbf{1}_{OX}$ and CPET for $\mathbf{2}_{OX}$. This linear relationship between $\Delta\Delta G^{\ddagger}$ values and the BDE values of the C−H bonds is consistent with the results of kinetic analyses summarized in Table 2: Complexes $\mathbf{1}_{OX}$ and $\mathbf{2}_{OX}$ showed close k values in oxidation of C−H bond having smaller BDE values, whereas $\mathbf{1}_{OX}$ showed much higher k values than those of $\mathbf{2}_{OX}$ in oxidation of C−H bonds having larger BDE values. Judging from the relation between oxidation activities and BDE values, and from the fact that only $\mathbf{1}_{OX}$ can oxidize ethylbenzene, it is assumed that $\mathbf{1}_{OX}$, which shows a

DOI: 10.1021/jacs.6b03785
J. Am. Chem. Soc. 2016, 138, 9508−9520

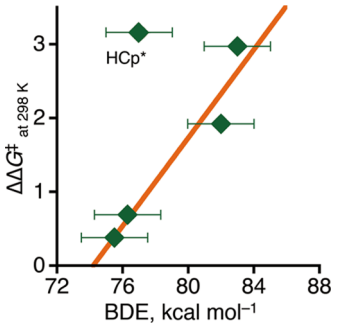

Figure 11. Plots of the differences in $\Delta G^{\ddagger}$ ($\Delta\Delta G^{\ddagger} = \Delta G^{\ddagger}(\mathbf{2}_{OX}) - \Delta G^{\ddagger}(\mathbf{1}_{OX})$) values for oxidation of the five hydrocarbon substrates between reaction with $\mathbf{1}_{OX}$ and $\mathbf{2}_{OX}$ at 298 K in MeCN against BDE values of C−H bonds to be cleaved in the substrates. In the linear fitting, the $\Delta\Delta G^{\ddagger}$ value for oxidation of HCp* is not included for the calculations.

higher BDE value than that of $\mathbf{2}_{OX}$, possesses higher activity for C−H abstraction than $\mathbf{2}_{OX}$.

CONCLUSIONS

The two Ru^{II}-pterin complexes employed in this work, **1** and **2**, have similar structures to each other, and their corresponding $1e^-$-oxidized species ($\mathbf{1}_{OX}$ and $\mathbf{2}_{OX}$) show relatively comparable BDE values in the thermochemical square schemes of PCET. Complexes $\mathbf{1}_{OX}$ and $\mathbf{2}_{OX}$ have difference in electron-acceptability and basicity; i.e., complex $\mathbf{1}_{OX}$ shows higher electron-acceptability than that of $\mathbf{2}_{OX}$, whereas complex $\mathbf{2}_{OX}$ shows higher basicity than $\mathbf{1}_{OX}$. To explore the impact of the electron-acceptability and basicity of the oxidant on the oxidation activity, the substrate oxidations with $\mathbf{1}_{OX}$ and $\mathbf{2}_{OX}$ were investigated on the basis of detailed kinetic analysis. Complexes $\mathbf{1}_{OX}$ and $\mathbf{2}_{OX}$ show the same reactivity in oxidation of substrates with relatively small BDE values such as xanthene, whereas in oxidation reactions of substrates with relatively large BDE values such as indene, complex $\mathbf{1}_{OX}$ showed a ca. 50 times larger rate constant than that with $\mathbf{2}_{OX}$, as reflected on the relationship between $\Delta\Delta G^{\ddagger}$ and BDEs of C−H bonds of the substrates. BEP analysis for the oxidation reaction with $\mathbf{1}_{OX}$ and $\mathbf{2}_{OX}$ and the DFT calculations revealed that complex $\mathbf{2}_{OX}$ attracts proton from the C−H bond of a substrate to make the bond more polarized for making electron transfer from the substrate more favorable. Therefore, pK_a and $E_{1/2}$ values of an oxidant are not only components of BDE as given in eq 1, but also are significant factors to control the reactivity of the oxidant as a hydrogen-atom acceptor by affecting the transition-state structure in CPET oxidation reactions.

ASSOCIATED CONTENT

Supporting Information

The Supporting Information is available free of charge on the ACS Publications website at DOI: 10.1021/jacs.6b03785.

Procedure of pK_a determination, DFT calculations, absorbance changes upon acid titration, crystal packing, electrochemical data, UV−vis spectral change upon oxidation of **2**, UV−vis and ESR spectral changes in oxidation reactions, spin-trapping ESR spectra, linear dependence of pseudo-first-order rate constants for substrate oxidation on the concentration of the substrate, Eyring plots, and tables of atomic coordinates for DFT-optimized structures. (PDF)

Complete crystallographic data for the complexes **2** and **2**-H^+. (ZIP)

AUTHOR INFORMATION

Corresponding Author

*kojima@chem.tsukuba.ac.jp

Notes

The authors declare no competing financial interest.

ACKNOWLEDGMENTS

This work was supported by Grants-in-Aids (No 24245011 and 15H00915 (T. K.) and 26-2583 (H. M.)) from the Japan Society of Promotion of Science (JSPS, MEXT) of Japan. Financial supports are also appreciated from The Mitsubishi Foundation and Yazaki Memorial Foundation for Science and Technology. We appreciate Prof. Masa-aki Ichinohe (University of Tsukuba) for his kind help in GC-EI MS measurements.

REFERENCES

(1) (a) Huynh, M. H. V.; Meyer, T. J. *Chem. Rev.* **2007**, *363*, 1246. (b) Warren, J. J.; Tronic, T. A.; Mayer, J. M. *Chem. Rev.* **2010**, *110*, 6961. (c) Gagliardi, C. J.; Westlake, B. C.; Kent, C. A.; Paul, J. J.; Papanikolas, J. M.; Meyer, T. J. *Coord. Chem. Rev.* **2010**, *254*, 2459. (d) Weinberg, D. R.; Gagliardi, C. J.; Hull, J. F.; Murphy, C. F.; Kent, C. A.; Westlake, B. C.; Paul, A.; Ess, D. H.; McCafferty, D. G.; Meyer, T. J. *Chem. Rev.* **2012**, *112*, 4016.

(2) (a) Mayer, J. M. *Annu. Rev. Phys. Chem.* **2004**, *55*, 363. (b) Hammes-Schiffer, S. *Acc. Chem. Res.* **2009**, *42*, 1881. (c) Hammes-Schiffer, S.; Hatcher, E.; Ishikita, H.; Skone, J. H.; Soudackov, A. V. *Coord. Chem. Rev.* **2008**, *252*, 384.

(3) Olah, G. A.; Molnár, Á. *Hydrocarbon Chemistry*; Wiley: New York, 1995.

(4) Snider, B. B. *Chem. Rev.* **1996**, *96*, 339.

(5) Reece, S. Y.; Nocera, D. G. *Annu. Rev. Biochem.* **2009**, *78*, 673.

(6) (a) Samuelsson, B.; Dahlè, S.-E.; Lindgren, J. Å.; Rouzer, C. A.; Serhan, C. N. *Science* **1987**, *237*, 1171. (b) Gradner, H. W. *Biochim. Biophys. Acta, Lipids Lipid Metab.* **1991**, *1084*, 221. (c) Clark, K. B.; Culshaw, P. N.; Griller, D.; Lossing, F. P.; Simões, J. A. M.; Walton, J. C. *J. Org. Chem.* **1991**, *56*, 5535. (d) de Groot, J. J. M. C.; Veldink, G. A.; Vliegenthart, J. F. G.; Boldingh, J.; Wever, R.; van Gelder, B. F. *Biochim. Biophys. Acta* **1975**, *377*, 71. (e) Schilstra, M. J.; Veldink, G. A.; Vliegenthart, J. F. G. *Biochemistry* **1994**, *33*, 3974. (f) Nelson, M. J. *J. Am. Chem. Soc.* **1988**, *110*, 2985.

(7) (a) Merkx, M.; Kopp, D. A.; Sazinsky, M. H.; Blazyk, J. L.; Müller, J.; Lippard, S. J. *Angew. Chem., Int. Ed.* **2001**, *40*, 2782. (b) Baik, M.-H. H.; Newcomb, M.; Friesner, R. A.; Lippard, S. J. *Chem. Rev.* **2003**, *103*, 2385.

(8) Mulliez, E.; Fontecave, M. *Chem. Ber.* **1997**, *130*, 317.

(9) Ortiz de Montellano, P. R. *Cytochrome P450 Structure, Mechanism, and Biochemistry*, 2nd ed.; Springer Science & Business Media, 1995.

(10) Du Bois, J.; Mizoguchi, T. J.; Lippard, S. J. *Coord. Chem. Rev.* **2000**, *200−202*, 443.

(11) Que, L., Jr.; Dong, Y. *Acc. Chem. Res.* **1996**, *29*, 190.

(12) (a) Groves, J. T.; Nemo, T. E.; Myers, R. S. *J. Am. Chem. Soc.* **1979**, *101*, 1032. (b) Groves, J. T.; Haushalter, R. C.; Nakamura, M.; Nemo, T. E.; Evans, B. J. *J. Am. Chem. Soc.* **1981**, *103*, 2884.

(13) (a) Cukier, R. I. *Biochim. Biophys. Acta, Bioenerg.* **2004**, *1655*, 37. (b) Hammes-Schiffer, S. *Acc. Chem. Res.* **2001**, *34*, 273.

(14) McMillen, D. F.; Golden, D. M. *Annu. Rev. Phys. Chem.* **1982**, *33*, 493.

(15) Tilset, M.; Parker, V. D. *J. Am. Chem. Soc.* **1989**, *111*, 6711.

(16) Parker, V. D.; Handoo, K. L.; Roness, F.; Tilset, M. *J. Am. Chem. Soc.* **1991**, *113*, 7493.

(17) Wayner, D. D.; Parker, V. D. *Acc. Chem. Res.* **1993**, *26*, 287.

(18) Skagestad, V.; Tilset, M. *J. Am. Chem. Soc.* **1993**, *115*, 5077.

DOI: 10.1021/jacs.6b03785
J. Am. Chem. Soc. 2016, 138, 9508−9520

(19) Tilset, M. In *Electron Transfer in Chemistry*; Balzani, V., Ed.; Wiley-VCH: Weinheim, Germany, 2001; Vol. 2, pp 677−713.
(20) (a) Mayer, J. M. *Acc. Chem. Res.* **2011**, *44*, 36. (b) Que, L., Jr. *Acc. Chem. Res.* **2007**, *40*, 493. (c) Nam, W. *Acc. Chem. Res.* **2007**, *40*, 522. (d) Fukuzumi, S. *Dalton Trans.* **2015**, *44*, 6696. (e) Ishizuka, T.; Ohzu, S.; Kojima, T. *Synlett* **2014**, *25*, 1667.
(21) Sastri, C. V.; Lee, J.; Oh, K.; Lee, Y. J.; Lee, J.; Jackson, T. A.; Ray, K.; Hirao, H.; Shin, W.; Halfen, J. A.; Kim, J.; Que, L., Jr.; Shaik, S.; Nam, W. *Proc. Natl. Acad. Sci. U. S. A.* **2007**, *104*, 19181.
(22) (a) Ohzu, S.; Ishizuka, T.; Hirai, Y.; Jiang, H.; Sakaguchi, M.; Ogura, T.; Fukuzumi, S.; Kojima, T. *Chem. Sci.* **2012**, *3*, 3421. (b) Takahashi, A.; Yamaki, D.; Ikemura, K.; Kurahashi, T.; Ogura, T.; Hada, M.; Fujii, H. *Inorg. Chem.* **2012**, *51*, 7296. (c) Rydberg, P.; Sigfridsson, E.; Ryde, U. *J. Biol. Inorg. Chem.* **2004**, *9*, 203.
(23) Groves, J. T.; Gross, Z.; Stern, M. K. *Inorg. Chem.* **1994**, *33*, 5065.
(24) Gupta, R.; Borovik, A. S. *J. Am. Chem. Soc.* **2003**, *125*, 13234.
(25) Usharani, D.; Lacy, D. C.; Borovik, A. S.; Shaik, S. *J. Am. Chem. Soc.* **2013**, *135*, 17090.
(26) (a) Roth, J. P.; Mayer, J. M. *Inorg. Chem.* **1999**, *38*, 2760. (b) Bryant, J. R.; Taves, J. E.; Mayer, J. M. *Inorg. Chem.* **2002**, *41*, 2769. (c) Lockwood, M. A.; Blubaugh, T. J.; Collier, A. M.; Lovell, S.; Mayer, J. M. *Angew. Chem., Int. Ed.* **1999**, *38*, 225. (d) Yuasa, J.; Fukuzumi, S. *J. Phys. Org. Chem.* **2008**, *21*, 886.
(27) Mader, E. A.; Davidson, E. R.; Mayer, J. M. *J. Am. Chem. Soc.* **2007**, *129*, 5153.
(28) (a) Manner, V. W.; DiPasquale, A. G.; Mayer, J. M. *J. Am. Chem. Soc.* **2008**, *130*, 7210. (b) Manner, V. W.; Mayer, J. M. *J. Am. Chem. Soc.* **2009**, *131*, 9874.
(29) (a) Hille, R. *Chem. Rev.* **1996**, *96*, 2757. (b) Kappock, T. J.; Caradonna, J. P. *Chem. Rev.* **1996**, *96*, 2659.
(30) (a) Benkovic, S. J.; Sammons, D.; Armarego, W. L. F.; Waring, P.; Inners, R. *J. Am. Chem. Soc.* **1985**, *107*, 3706. (b) Bobst, A. *Helv. Chim. Acta* **1967**, *50*, 2222.
(31) Kaim, W.; Schwederski, B.; Heilmann, O.; Hornung, F. M. *Coord. Chem. Rev.* **1999**, *182*, 323.
(32) (a) Abelleira, A.; Galang, R. D.; Clarke, M. J. *Inorg. Chem.* **1990**, *29*, 633. (b) Kohzuma, T.; Masuda, H.; Yamauchi, O. *J. Am. Chem. Soc.* **1989**, *111*, 3431. (c) Odani, A.; Masuda, H.; Inukai, K.; Yamauchi, O. *J. Am. Chem. Soc.* **1992**, *114*, 6294. (d) Kojima, T.; Sakamoto, T.; Matsuda, Y.; Ohkubo, K.; Fukuzumi, S. *Angew. Chem., Int. Ed.* **2003**, *42*, 4951. (e) Inui, Y.; Miyazaki, S.; Ohkubo, K.; Fukuzumi, S.; Kojima, T. *Angew. Chem., Int. Ed.* **2012**, *51*, 4623.
(33) Miyazaki, S.; Kojima, T.; Sakamoto, T.; Matsuyama, T.; Ohkubo, K.; Fukuzumi, S. *Inorg. Chem.* **2008**, *47*, 333.
(34) Miyazaki, S.; Kojima, T.; Mayer, J. M.; Fukuzumi, S. *J. Am. Chem. Soc.* **2009**, *131*, 11615.
(35) Wong, Y.-L.; Mak, C.-Y.; Kwan, H. S.; Lee, H. K. *Inorg. Chim. Acta* **2010**, *363*, 1246.
(36) Luo, J.; Rath, N. P.; Mirica, L. M. *Inorg. Chem.* **2011**, *50*, 6152.
(37) Yamauchi, O.; Odani, A.; Masuda, H.; Funahashi, Y. In *Bioinorganic Chemistry of Copper*; Karlin, K. D., Tyeklár, Z., Eds.; Chapman & Hall: New York, 1993; p 363.
(38) Shimizu, Y.; Fukui, S.; Oi, T.; Nagao, H. *Bull. Chem. Soc. Jpn.* **2008**, *81*, 1285.
(39) Goldsmith, C. R.; Jonas, R. T.; Stack, T. D. P. *J. Am. Chem. Soc.* **2002**, *124*, 83.
(40) Connelly, N. G.; Geiger, W. E. *Chem. Rev.* **1996**, *96*, 877.
(41) Buettner, G. R. *Free Radical Biol. Med.* **1987**, *3*, 259.
(42) Kabuto, C.; Akine, S.; Nemoto, T.; Kwon, E. *Nippon Kessho Gakkaishi* **2009**, *51*, 218.
(43) *CRC Handbook of Chemistry and Physics*, 82nd ed.; CRC Press, Boca Raton, 2001; Section 9.
(44) Miyazaki, S.; Ohkubo, K.; Kojima, T.; Fukuzumi, S. *Angew. Chem., Int. Ed.* **2008**, *47*, 9669.
(45) (a) Aakeröy, C. B.; Evans, T. A.; Seddon, K. R.; Pálinko, I. *New J. Chem.* **1999**, *23*, 145. (b) Jones, P. G.; Ahrens, P. *Chem. Commun.* **1998**, 2307.
(46) Kaljurand, I.; Kütt, A.; Sooväli, L.; Rodima, T.; Mäemets, V.; Leito, I.; Koppel, I. A. *J. Org. Chem.* **2005**, *70*, 1019.
(47) Izutsu, K. *Acid-Base Dissociation Constants in Dipolar Aprotic Solvents*; Blackwell Scientific: Boston, MA, 1990.
(48) The pK_a value of **1**-H$^+$ was previously reported to be 15.7 in ref 34. This value has been corrected.
(49) Wu, A.; Mayer, J. M. *J. Am. Chem. Soc.* **2008**, *130*, 14745.
(50) Mader, E. A.; Manner, V. W.; Markle, T. F.; Wu, A.; Franz, J.; Mayer, J. M. *J. Am. Chem. Soc.* **2009**, *131*, 4335.
(51) The BDE value for **1**-H$^+$ has been recalculated to be 85 kcal mol^{-1} on the basis of the pK_a value of 14.3 and eq 1.
(52) Rhile, J. I.; Markle, T. F.; Nagano, H.; Dipasquale, A. G.; Lam, O. P.; Lockwood, M. A.; Rotter, K.; Mayer, J. M. *J. Am. Chem. Soc.* **2006**, *128*, 6075.
(53) Manna, B.; Ghosh, R.; Oalit, D. K. *J. Phys. Chem. C* **2015**, *119*, 10641.
(54) The absorption spectrum of **1**-H$^+$ has been reported to show the absorption maxima (ε [M^{-1} cm^{-1}]) at 490 (8.0×10^3) and 441 (1.0×10^4) nm. See ref 34.
(55) (a) Bordwell, F. G.; Cheng, J.-P.; Ji, G.-Z.; Satish, A. V.; Zhang, X. *J. Am. Chem. Soc.* **1991**, *113*, 9790. (b) Bordwell, F. G. *Acc. Chem. Res.* **1988**, *21*, 456.
(56) Luo, Y.-R. *Handbook of Bond Dissociation Energies in Organic Compounds*; CRC Press: Boca Raton, 2003.
(57) Marcinek, A.; Rogowski, J.; Adamus, J.; Gębicki, J.; Platz, S. *J. Phys. Chem.* **1996**, *100*, 13539.
(58) Akbulut, U.; Khurshid, A.; Hacioğlu, B.; Toppare, L. *Polymer* **1990**, *31*, 1343.
(59) (a) Barr, D. P.; Gunther, M. R.; Deterding, L. J.; Tomer, K. B.; Mason, R. P. *J. Biol. Chem.* **1996**, *271*, 15498. (b) Aljuhani, N.; Whittal, R. M.; Khan, S. R.; Siraki, A. G. *Chem. Res. Toxicol.* **2015**, *28*, 1476.
(60) Matsumoto, T.; Ohkubo, K.; Honda, K.; Yazawa, A.; Furutachi, H.; Fujinami, S.; Fukuzumi, S.; Suzuki, M. *J. Am. Chem. Soc.* **2009**, *131*, 9258.
(61) (a) Stoyanovsky, D. A.; Melnikov, Z.; Cederbaum, A. I. *Anal. Chem.* **1999**, *71*, 715. (b) McCormick, M. L.; Buettner, G. R.; Britigan, B. E. *J. Biol. Chem.* **1995**, *279*, 29265. (c) Huling, S. G.; Arnold, R. G.; Sierka, R. A.; Miller, M. R. *Environ. Sci. Technol.* **1998**, *32*, 3436.
(62) Bryant, J. R.; Mayer, J. M. *J. Am. Chem. Soc.* **2003**, *125*, 10351.
(63) In accordance with description in ref 2a, we compared the measured activation barriers ($\Delta G^{\ddagger}$) in the DHA oxidation reactions by $\mathbf{1}_{OX}$ (13.9 kcal mol^{-1}) and $\mathbf{2}_{OX}$ (14.6 kcal mol^{-1}) to the estimated free energy differences for ET (ΔG°_{ET} = 39.4 kcal mol^{-1} for $\mathbf{1}_{OX}$ and 49.1 kcal mol^{-1} for $\mathbf{2}_{OX}$) and those for PT (ΔG°_{PT} = 42.6 kcal mol^{-1} for $\mathbf{1}_{OX}$ and 40.7 kcal mol^{-1} for $\mathbf{2}_{OX}$). The $\Delta G^{\ddagger}$ values are smaller than the ΔG°_{ET} and ΔG°_{PT} values, and thus the concerted mechanism for the substrate oxidation with $\mathbf{1}_{OX}$ and $\mathbf{2}_{OX}$ has been further confirmed.
(64) (a) Roecker, L. E.; Meyer, T. J. *J. Am. Chem. Soc.* **1987**, *109*, 746. (b) Thompson, M. S.; Meyer, T. J. *J. Am. Chem. Soc.* **1982**, *104*, 4106. (c) Stultz, L. K.; Huynh, M. H. V.; Binstead, R. A.; Curry, M.; Meyer, T. J. *J. Am. Chem. Soc.* **2000**, *122*, 5984.
(65) (a) Kotani, H.; Kaida, S.; Ishizuka, T.; Sakaguchi, M.; Ogura, T.; Shiota, Y.; Yoshizawa, K.; Kojima, T. *Chem. Sci.* **2015**, *6*, 945. (b) Morimoto, Y.; Park, J.; Suenobu, T.; Lee, Y.-M.; Nam, W.; Fukuzumi, S. *Inorg. Chem.* **2012**, *51*, 10025.
(66) Mayer, J. M. *Acc. Chem. Res.* **1998**, *31*, 441.
(67) Wang, D.; Zhang, M.; Bühlmann, P.; Que, L., Jr. *J. Am. Chem. Soc.* **2010**, *132*, 7638.
(68) Goldsmith, C. R.; Cole, A. P.; Stack, T. D. P. *J. Am. Chem. Soc.* **2005**, *127*, 9904.
(69) Goldsmith, C. R.; Stack, T. D. P. *Inorg. Chem.* **2006**, *45*, 6048.
(70) To compare the reactivity of complex $\mathbf{1}_{OX}$ in the O−H and C−H oxidation, the log k' values at 296 K for oxidation of six phenol derivatives (ref 34) and six hydrocarbons (this work) with $\mathbf{1}_{OX}$ were plotted against BDE values of the O−H and C−H bonds to be cleaved in the substrates (Figure S18). Except the HCp* oxidation, the C−H and O−H oxidations showed different dependence on the BDE values of the substrates; the rate constant of the O−H oxidation was larger than that of the C−H oxidation at the same BDE value. However, the

DOI: 10.1021/jacs.6b03785
J. Am. Chem. Soc. 2016, 138, 9508−9520

slopes of the BDE dependence are almost the same for the C−H and O−H oxidation (α = −0.27 for the C−H oxidation and −0.29 for the O−H oxidation). Therefore, we conclude that complex $\mathbf{1}_{OX}$ can oxidize both C−H and O−H bonds in the same CPET mechanism.

(71) (a) Leffler, J. E. *Science* **1953**, *117*, 340. (b) Murdoch, J. R. *J. Am. Chem. Soc.* **1972**, *94*, 4410.

(72) (a) Garrera, H. A.; Gsponer, H. E.; Garcia, N. A.; Cosa, J. J.; Previtali, C. M. *J. Photochem.* **1986**, *33*, 257. (b) Garrera, H. A.; Cosa, J. J.; Previtali, C. M. *J. Photochem. Photobiol., A* **1991**, *56*, 267.

(73) Bader, J. S.; Kuharski, R. A.; Chandler, D. *J. Chem. Phys.* **1990**, *93*, 230.

(74) Ungar, L. W.; Newton, M. D.; Voth, G. A. *J. Phys. Chem. B* **1999**, *103*, 7367.

DOI: 10.1021/jacs.6b03785
J. Am. Chem. Soc. 2016, 138, 9508−9520